ISSN 2072-5981

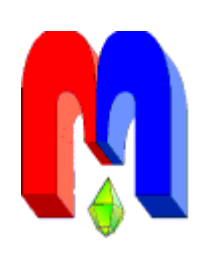


Volume 27
Issue 3
Article No 25303
1-11 pages
2025

doi: 10.26907/mrsej-25303

http://mrsej.kpfu.ru

http://mrsej.elpub.ru



Established and published by Kazan University*
Endorsed by International Society of Magnetic Resonance (ISMAR)
Registered by Russian Federation Committee on Press (#015140),
August 2, 1996
First Issue appeared on July 25, 1997

© Kazan Federal University (KFU)[†]

"Magnetic Resonance in Solids. Electronic Journal" (MRSej) is a peer-reviewed, all electronic journal, publishing articles which meet the highest standards of scientific quality in the field of basic research of a magnetic resonance in solids and related phenomena.

Indexed and abstracted by

Web of Science (ESCI, Clarivate Analytics, from 2015), White List (from 2023) Scopus (Elsevier, from 2012), RusIndexSC (eLibrary, from 2006), Google Scholar, DOAJ, ROAD, CyberLeninka (from 2006), SCImago Journal & Country Rank, etc.

Editor-in-Chief

Boris Kochelaev (KFU, Kazan)

Executive Editor Yurii **Proshin** (KFU, Kazan) mrsej@kpfu.ru

Honorary Editors

Jean Jeener (Universite Libre de Bruxelles, Brussels) Raymond **Orbach** (University of California, Riverside)



This work is licensed under a Creative Commons Attribution-ShareAlike 4.0 International License.

This is an open access journal which means that all content is freely available without charge to the user or his/her institution. This is in accordance with the BOAI definition of open access.

Technical Editor
Maxim Avdeev (KFU, Kazan)
mrsej@kpfu.ru

Editors

Vadim **Atsarkin** (Institute of Radio Engineering and Electronics, Moscow)
Yurij **Bunkov** (CNRS, Grenoble)
Mikhail **Eremin** (KFU, Kazan)
David **Fushman** (University of Maryland, College Park)
Hugo **Keller** (University of Zürich, Zürich)

Yoshio **Kitaoka** (Osaka University, Osaka)

Boris **Malkin** (KFU, Kazan) Alexander **Shengelaya** (Tbilisi State University, Tbilisi)

Jörg **Sichelschmidt** (Max Planck Institute for Chemical Physics of Solids, Dresden)

Haruhiko **Suzuki** (Kanazawa University, Kanazava) Murat **Tagirov** (KFU, Kazan) Dmitrii **Tayurskii** (KFU, Kazan) Valentine **Zhikharev** (KNRTU, Kazan)

^{*} Address: "Magnetic Resonance in Solids. Electronic Journal", Kazan Federal University; Kremlevskaya str., 18; Kazan 420008, Russia

[†] In Kazan University the Electron Paramagnetic Resonance (EPR) was discovered by Zavoisky E.K. in 1944.

Magnetic properties of high entropy compound $Ca_{0.25}Sr_{0.5}La_{0.25}Mn_{0.5}Ti_{0.5}O_3$

I.V. Yatsyk^{1*}, D.V. Popov¹, R.F. Likerov¹, R.G. Batulin², M.A. Cherosov², A.V. Khusanzyanov², R.M. Eremina¹

 $^1\mathrm{Zavoisky}$ Physical-Technical Institute, FRC Kazan Scientific Center of RAS, 420029 Kazan, Russia

²Kazan Federal University, 420008 Kazan, Russia

*E-mail: i.yatzyk@gmail.com

(received September 28, 2025; revised October 14, 2025; accepted October 24, 2025; published October 27, 2025)

This work presents the first comprehensive study of the magnetic properties of the novel perovskite-type high-entropy oxide $\text{Ca}_{0.25}\text{Sr}_{0.5}\text{La}_{0.25}\text{Mn}_{0.5}\text{Ti}_{0.5}\text{O}_3$. A polycrystalline powder of the compound was synthesized using the solid-state reaction method. The compound crystallizes in the tetragonal system with space group I4/mcm and lattice parameters $a=b=5.48320\,\text{Å}$, $c=7.74480\,\text{Å}$, and $\alpha=\beta=\gamma=90^\circ$. The homogeneity and uniform distribution of the constituent elements were confirmed by X-ray fluorescence analysis. The emergence of magnetic ordering at $\approx 40\,\text{K}$ is evidenced by a maximum in the temperature-dependent ESR integrated intensity, coinciding with the divergence of the ZFC/FC magnetization curves. The ESR spectrum itself is well fitted by four lines. A second, distinct phase transition is observed at approximately 300 K. Magnetization hysteresis loops measured below room temperature exhibit weak ferromagnetic behavior, with the coercive field increasing to 750 Oe at 5 K. The sign reversal of the Seebeck coefficient at $T\approx 475\,\text{K}$ indicates a change in the conductivity type of the compound. The temperature dependence of the sample's conductivity was described within the small polariton hopping model, and the activation energy was 269 meV.

PACS: 71.70.Ch, 75.10.Dg, 76.30.Kg, 71.70.Ej.

Keywords: High entropy manganite; Exchange interaction; Magnetic phase transition; ESR; Magnetization

1. Introduction

Complex perovskite oxides with the general formula ABO₃ remain a focus of intensive research due to their diverse physical properties, including magnetism, ferroelectricity, and thermoelectricity, as well as the intricate interplay between them [1–3]. The ability to tailor these properties through targeted ionic substitution at the A- and B-sites of the structure offers promising avenues for designing materials with specific functional characteristics. Particular relevance lies in the co-doping of magnetic and non-magnetic ions at the B-site, which can significantly alter the magnetic order and enhance thermoelectric efficiency. In this context, compounds containing both magnetic manganese (Mn) and titanium (Ti) ions are of special interest, as their mixed valence states and complex electron interactions are key to understanding the mechanisms governing magnetic and electronic behavior.

High-entropy compounds, featuring multiple principal elements on the A and B sites, represent a promising direction within this field, as discussed in recent reviews [4, 5]. For such complex compositions, structural stability is a critical prerequisite. This stability in perovskites is commonly assessed using the Goldschmidt tolerance factor, which serves as a predictor for the formation and stability of the perovskite structure [6]. The structural features of a perovskite are

determined by the Goldschmidt tolerance factor, which predicts the stability of the structure [6]:

$$t = \frac{R_{\rm A} + R_{\rm O}}{\sqrt{2}(R_{\rm B} + R_{\rm O})},\tag{1}$$

where R_A , R_B , and R_O are the ionic radii of the A-site cation, B-site cation, and oxygen anion, respectively. A cubic perovskite structure is typically stable for $0.9 \le t \le 1.0$. Values of t > 1.0 often lead to hexagonal or tetragonal phases, while t < 0.9 favors the formation of orthorhombic or rhombohedral structures. The Goldschmidt tolerance factor allows for a preliminary assessment of geometric stability, indicating a comparable probability of perovskite formation for systems with similar t values.

When the A-site is occupied by up to five different elements, an additional criterion is required to evaluate the structural stability. This is characterized by the quenched disorder arising from the A-site cation size mismatch, quantified by the disorder parameter σ [7]:

$$\sigma^2 = \sum x_i R_i^2 - \langle R_A \rangle^2 \,, \tag{2}$$

where

$$\langle R_A \rangle = \sum x_i R_i. \tag{3}$$

A high value of σ indicates the possibility of the formation of small ferromagnetic clusters, a deviation of the susceptibility from Curie-Weiss behavior above $T_{\rm C}$, and the realization of the Griffiths phase scenario.

Perovskite-type manganites with the general formula $RE_{1-x}AE_xMnO_3$ (where RE is a rareearth ion and AE is an alkaline-earth ion) are important strongly correlated electron systems. They exhibit a range of remarkable phenomena, including colossal magnetoresistance (CMR), electronic phase separation, and metal-insulator transitions.

The substitution of cations on the A-site directly alters the valence state of manganese. Furthermore, doping with elements of different ionic radii effectively induces orthorhombic distortion, which modifies the Mn–O–Mn bond angle and Mn–O bond lengths. The distinctive magnetic properties of high-entropy manganites have been recently explored in studies such as [8,9].

The purpose of this work is to study the magnetic properties of the high-entropy perovskite compound $Ca_{0.25}Sr_{0.5}La_{0.25}Mn_{0.5}Ti_{0.5}O_3$.

2. Sample preparation

The design of a high-entropy perovskite oxide with high thermal stability requires consideration of both charge balance and geometric stability. Based on these criteria, the selection of A-site elements was restricted to cations with +2 (Ca, Sr) and +3 (La) valence states [10].

Polycrystalline $Ca_{0.25}Sr_{0.5}La_{0.25}Mn_{0.5}Ti_{0.5}O_3$ was synthesized via a solid-state reaction route using high-purity ($\geq 99\%$) precursors: $CaCO_3$, $SrCO_3$, La_2O_3 , TiO_2 , and Mn_2O_3 . The powders were mixed in a planetary mill with zirconia balls in ethanol. The resulting mixture was dried for 12 hours and subsequently calcined at 1323 K for 10 hours in air. The calcined powder was then pressed into pellets and sintered at 1373 K for 6 hours in air. Further details on the synthesis conditions can be found in references [1, 11, 12].

3. Results

3.1. XRF

The chemical composition of the single crystal was determined by X-ray fluorescence (XRF) analysis using a Bruker S2 Ranger spectrometer. The elemental distribution mapping (Fig.1) confirms a homogeneous distribution of all constituent elements throughout the sample. Quantitative analysis yielded the following cation ratios: Ca/La/Sr = 0.247/0.226/0.526 for the A-site and Ti/Mn = 0.485/0.515 for the B-site. Within experimental error, these ratios are consistent with the nominal stoichiometry of $\text{Ca}_{0.25}\text{Sr}_{0.5}\text{La}_{0.25}\text{Mn}_{0.5}\text{Ti}_{0.5}\text{O}_3$.

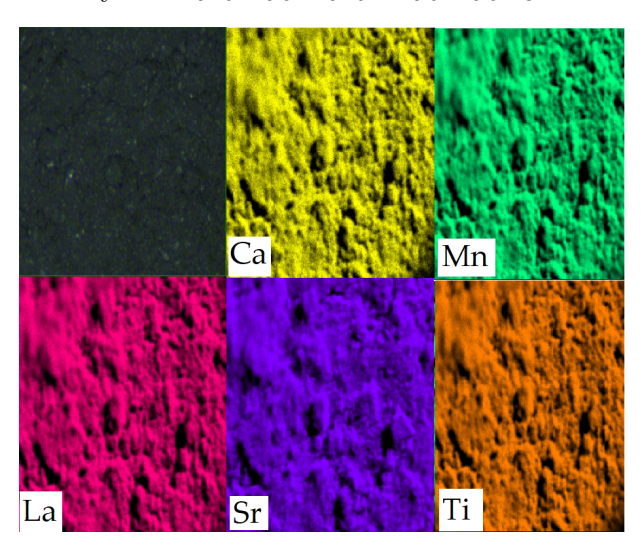


Figure 1. X-ray fluorescence analysis results for Ca_{0.25}Sr_{0.5}La_{0.25}Mn_{0.5}Ti_{0.5}O₃

3.2. XRD

X-ray diffraction (XRD) data were collected on a LAN Scientific FRINGE XRD-602 diffractometer operating at a tube power of 600 W. The data were acquired with a step size of 0.02° and an accumulation time of 1 s per step. Rietveld refinement of the diffraction patterns (Fig.2) confirms that the sample crystallizes in the tetragonal system with space group I4/mcm. The refined lattice parameters are a = b = 5.48320 Å, c = 7.74480 Å, $\alpha = \beta = \gamma = 90^{\circ}$. The crystal structure of Ca_{0.25}Sr_{0.5}La_{0.25}Mn_{0.5}Ti_{0.5}O₃ is illustrated in Fig.3.

3.3. ESR

Electron spin resonance (ESR) measurements were performed on a Bruker EMXPlus spectrometer operating at a frequency of 9.34 GHz. For the low-temperature range (5–120 K), an ESR900 helium cryostat (Oxford Instruments) with an ITC503S PID controller was used. Measurements in the higher temperature range (117–339 K) were conducted using an ER4131VT nitrogen purge system with a BVT3000 temperature controller. Both setups utilized an ER 4122SHQE cylindrical resonator (Bruker) with TE $_{011}$ microwave distribution.

The experimental spectra, along with their corresponding fits, are presented in Fig.4. The spectra were modeled using a superposition of four distinct lines. The shape of each line has been described by the equation in Ref. [13]:

$$\frac{dP}{dH} = \frac{d}{dH} \left(\frac{\Delta H + \alpha (H - H_{\text{res}})}{(H - H_{\text{res}})^2 + \Delta H^2} + \frac{\Delta H - \alpha (H + H_{\text{res}})}{(H + H_{\text{res}})^2 + \Delta H^2} \right),\tag{4}$$

where $H_{\rm res}$ is the resonance magnetic field, ΔH is the linewidth, and α is the asymmetry

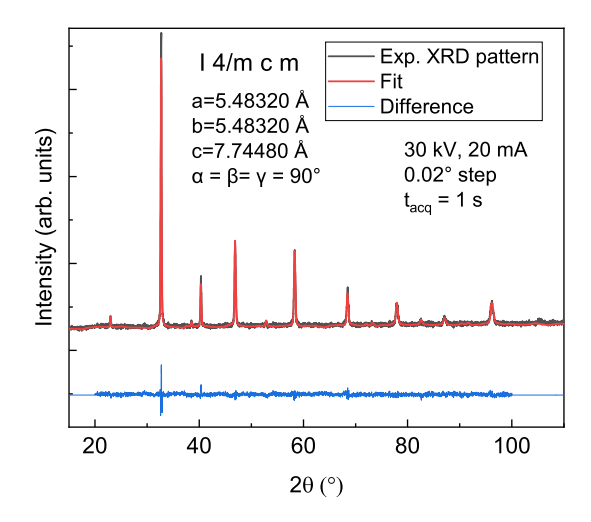


Figure 2. PXRD pattern and Rietveld refinement fit for Ca_{0.25}Sr_{0.5}La_{0.25}Mn_{0.5}Ti_{0.5}O₃

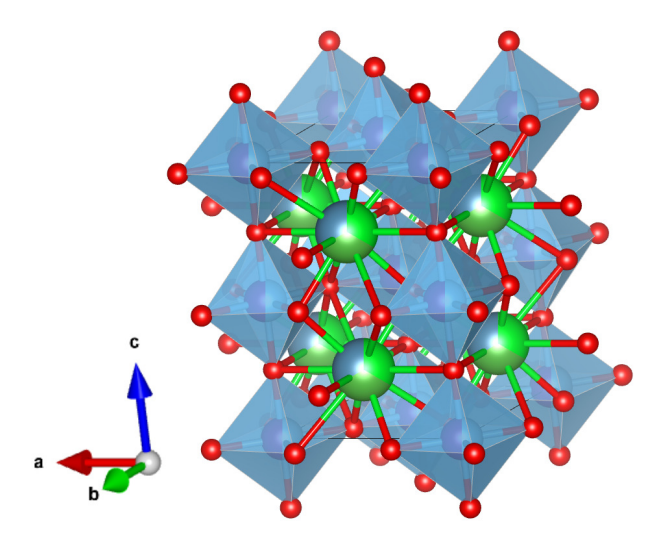


Figure 3. Crystal structure of Ca_{0.25}Sr_{0.5}La_{0.25}Mn_{0.5}Ti_{0.5}O₃. Blue octahedra represent the coordination environment of the B-site metal cations. Red spheres represent oxygen ions

parameter [14]. All fitted parameters exhibit a local extremum near $T=40\,\mathrm{K}$, suggesting a phase transition. A second anomaly is observed around 65 K, manifested as extrema in the linewidth and integrated intensity of two specific spectral lines (green and red line see Fig.5), which indicates a change in the magnetic order. Furthermore, the four spectral components merge into a single line at temperatures above 300 K.

3.4. Magnetization

Magnetization measurements were carried out with PPMS-9 Quantum Design device. Temperature dependence of the magnetization was measured in zero-field cooling (ZFC) and field cooling (FC) modes for the external magnetic field values of 0.1 and 1 kOe and temperature range of 5–380 K. The received lines reveal a phase transition at $T=40\,\mathrm{K}$ (Fig.6). In addition, lines exhibit curvature at $T\approx300\,\mathrm{K}$. Both temperatures are featured in ESR measurements.

Magnetization hysteresis loops were recorded at selected temperatures (5, 30, 45, 150, and 300 K) in applied fields up to ± 9 T. While weak hysteresis is observed at all temperatures, the

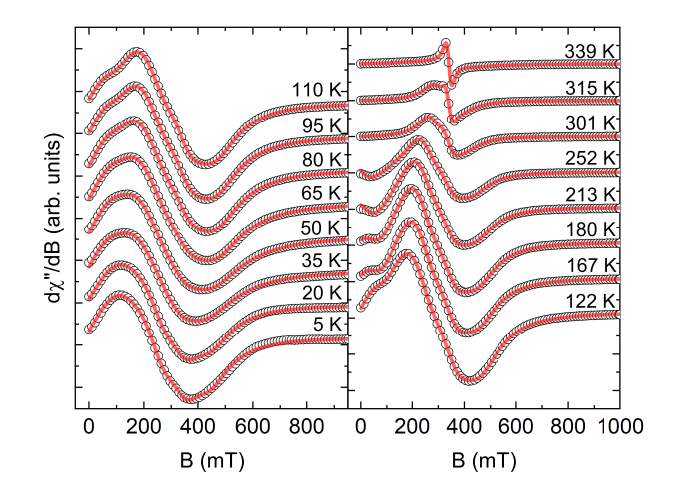


Figure 4. Evolution of the ESR spectra with temperature for Ca_{0.25}Sr_{0.5}La_{0.25}Mn_{0.5}Ti_{0.5}O₃. Open symbols show the experimental data, and solid lines are the fits. Spectra were recorded at a frequency of 9.34 GHz in the temperature range of 5–339 K

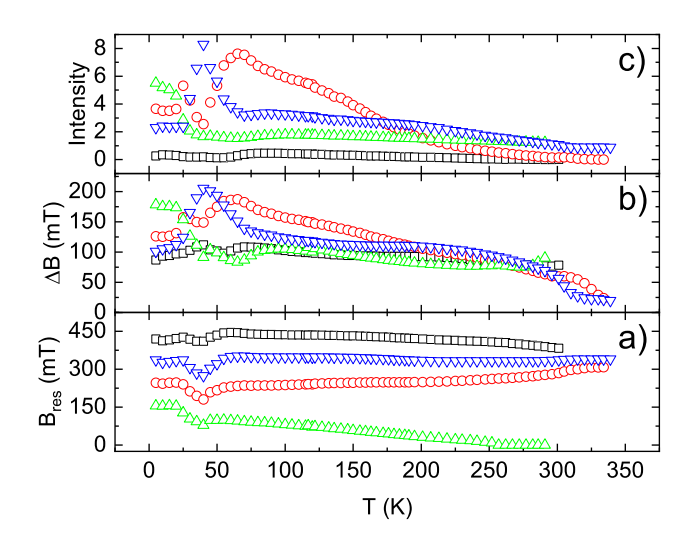


Figure 5. Temperature dependence of (a) the resonance magnetic field, (b) the linewidth, and (c) the integrated intensity of the four ESR lines for the Ca_{0.25}Sr_{0.5}La_{0.25}Mn_{0.5}Ti_{0.5}O₃ sample

loops exhibit a substantial increase in coercivity and remanent magnetization at $5 \,\mathrm{K}$ and $30 \,\mathrm{K}$. This enhancement is likely a consequence of the magnetic phase transition near $T = 40 \,\mathrm{K}$ (Fig.7).

3.5. Thermoelectricity

The Seebeck coefficient and electrical resistivity were measured from 300 to 800 K using a custom-built apparatus with a temperature gradient of $\Delta T = 30$ K. The temperature dependence of the Seebeck coefficient for Ca_{0.25}Sr_{0.5}La_{0.25}Mn_{0.5}Ti_{0.5}O₃ is shown in Fig.8. The observed behavior suggests contributions from charge carriers of different signs. The sign reversal of the Seebeck coefficient at $T \approx 475$ K indicates a change in the conductivity type of the compound (Fig.8). The temperature dependence of the resistivity is presented in an plot (ln(T/R) versus 1/T) in Fig.9.

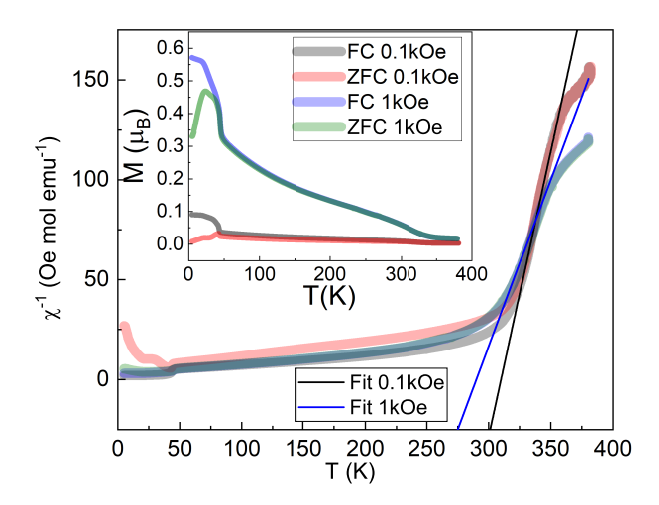


Figure 6. Temperature dependence of the inverse magnetic susceptibility $(1/\chi)$ for the $Ca_{0.25}Sr_{0.5}La_{0.25}Mn_{0.5}Ti_{0.5}O_3$ sample. The solid line represents the Curie-Weiss fit to the paramagnetic region. Inset: Temperature dependence of the magnetization

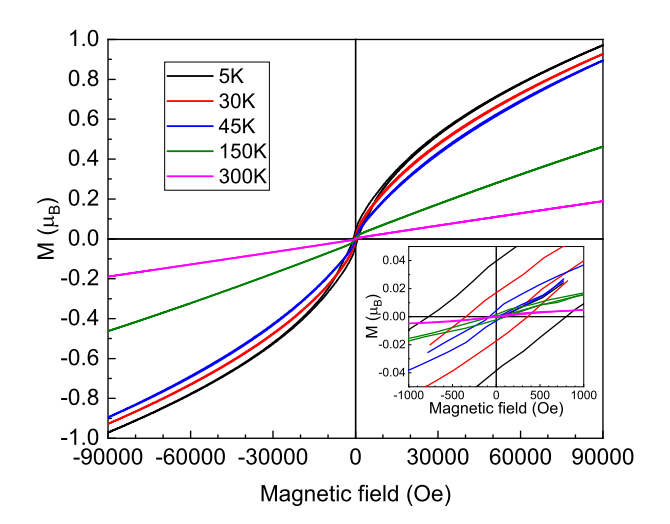


Figure 7. Magnetic field dependence of the magnetization of $Ca_{0.25}Sr_{0.5}La_{0.25}Mn_{0.5}Ti_{0.5}O_3$ sample. Inset: the low-field region is magnified to clearly display the hysteresis loops and quantify the coercivity

The resistivity data were fitted based on the small polaron hopping model, utilizing the relation [2]:

$$\frac{1}{R} \propto \frac{A}{T} \exp\left(-\frac{\Delta E}{k_{\rm B} T}\right),\tag{5}$$

where A is a constant and ΔE is the band gap. The obtained value of $269\pm3\,\mathrm{meV}$ (Fig.9) falls within the typical range for perovskite-type compounds [16,17].

4. Discussion

X-ray fluorescence analysis indicates that divalent cations (Ca^{2+} and Sr^{2+}) constitute approximately 75% of the A-site occupancy. To maintain charge neutrality, this necessitates that titanium ions adopt the Ti^{4+} state. Consequently, manganese ions must exhibit a mixed valence,

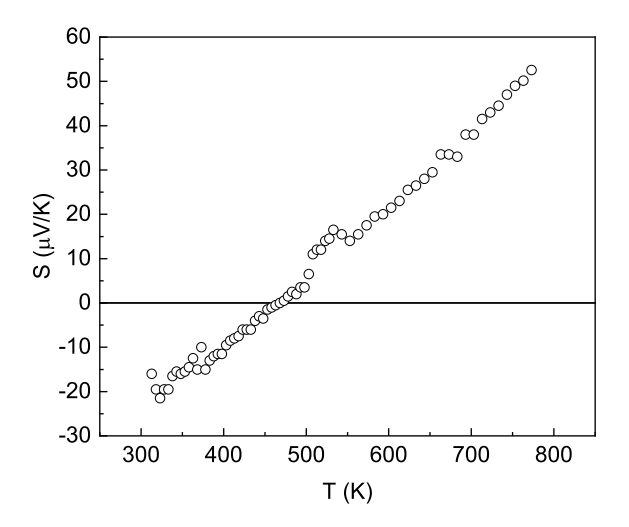


Figure 8. Temperature dependence of the Seebeck coefficient Ca_{0.25}Sr_{0.5}La_{0.25}Mn_{0.5}Ti_{0.5}O₃ sample

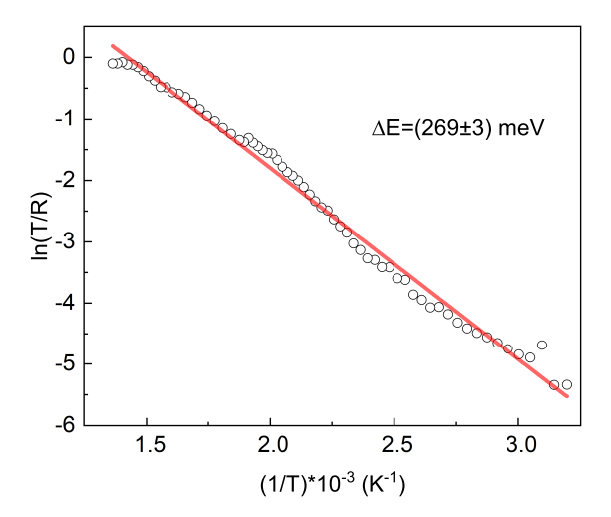


Figure 9. Temperature dependence of the electrical conductivity of $Ca_{0.25}Sr_{0.5}La_{0.25}Mn_{0.5}Ti_{0.5}O_3$. The logarithm of the conductivity, ln(T/R), is plotted as a function of inverse temperature, 1/T

with an equal distribution (50% each) of $\rm Mn^{3+}$ and $\rm Mn^{4+}$ states. This valence configuration satisfies the charge balance requirement for the compound $\rm Ca_{0.25}^{2+}Sr_{0.5}^{2+}La_{0.25}^{3+}Mn_{0.25}^{4+}Mn_{0.25}^{3+}Ti_{0.5}^{4+}O_3^{2-}$. For instance, the magnetic properties of the high-entropy manganite under study can be compared to those of the compound $\rm La_{0.5}^{3+}Sr_{0.5}^{2+}Mn_{0.5}^{4+}Mn_{0.5}^{3+}O_3^{2-}$. According to Zhang et al. [18], rigorous measurements of DC magnetization and isothermal magnetization confirm a paramagnetic-to-ferromagnetic phase transition at 340 K, with the formation of spontaneous magnetization below the Curie temperature ($T_{\rm C}$). The reported $T_{\rm C}$ for $\rm La_{0.5}Sr_{0.5}MnO_3$ is consistent with the temperature-dependent magnetization behavior observed in our high-entropy manganite.

The presence of multiple elements at the A-site alters the Mn–O–Mn bond angle, leading to distinctive features in the low-temperature magnetization behavior. A pertinent example is provided by the study of magnetization in $\text{La}_{0.5-y}\text{Y}_y\text{Sr}_{0.5}\text{MnO}_3$ [19]. It should be noted that as the yttrium concentration increases, the distortion of the MnO₆ octahedra increases. This results in the collapse of the long-range ferromagnetic order and the formation of a short-range

ordered state, which can be described in terms of magnetic clusters. Consequently, the ZFC magnetization curve begins to deviate from the FC curve. This is followed by a sharp peak in the ZFC magnetization at a temperature $T_{\rm SG}=40\,\rm K$, accompanied by a clear bifurcation between the ZFC and FC branches. This cusp at $T_{\rm SG}$ corresponds to the freezing temperature of the clusters, which originates from the frustration between the ferromagnetic (FM) order within the clusters and the antiferromagnetic (AFM) interactions present in the surrounding matrix.

Using Eq.1 for the tolerance factor and the ionic radii from Table 1, we calculated a value of t = 0.904 for the compound under study. This value is in good agreement with the I4/mcm tetragonal space group identified by X-ray analysis.

Ion	Coordination number	Radius (nm)
Ca^{2+}	8	0.112
Sr^{2+}	8	0.126
La ³⁺	8	0.116
$\mathrm{Mn^{3+}}$	6	0.0645
Mn^{4+}	6	0.068
Ti ⁴⁺	6	0.0605

Table 1. Radius of ions

The degree of disorder was also assessed using Eq.2. For an average A-site cation radius of $\langle r_A \rangle = 0.120156 \,\mathrm{nm}$, the calculated variance was $\sigma^2 = 5.27 \times 10^{-5} \,\mathrm{\mathring{A}}$.

Despite the structural stability and low degree of disorder, the system exhibits magnetic phase separation, as evidenced by magnetization data and magnetic resonance spectroscopy. At 340 K, the magnetic resonance spectrum consists of a single line. Upon cooling, this line broadens and splits into two components. The second component shifts toward lower magnetic fields down to 300 K. With a further decrease in temperature, the spectral shape can only be accurately described by considering four distinct lines.

We believe that the spectral line represented by the blue triangles (Fig.5) corresponds to the paramagnetic phase of the sample, which is characterized by antiferromagnetic exchange interactions between manganese spins. The integral intensity of this line increases with decreasing temperature, reaches a maximum at 40 K, and then drops sharply upon further cooling. Notably, features are also observed in the temperature-dependent magnetization (Fig.6) at this same temperature. We associate the three remaining magnetic resonance lines, represented in black, red, and green, with ferromagnetic regions within the sample.

On the other hand, the significant broadening of the ferromagnetic lines appears to be caused by anisotropic exchange interactions, such as single-ion anisotropy of the manganese ions and the Dzyaloshinskii-Moriya interaction. Using the methodology proposed by Griscom et al. [20], we estimated the temperature dependence of the anisotropic exchange interaction magnitude (see Fig.10). As shown in the figure, the anisotropy field increases nearly linearly with decreasing temperature down to approximately 50 K, below which it stabilizes at a constant value of about 1600 Oe. The order of magnitude of the obtained anisotropy field is consistent with values reported earlier for manganites [21].

The obtained temperature dependencies of the magnetic susceptibility (above 300 K) were

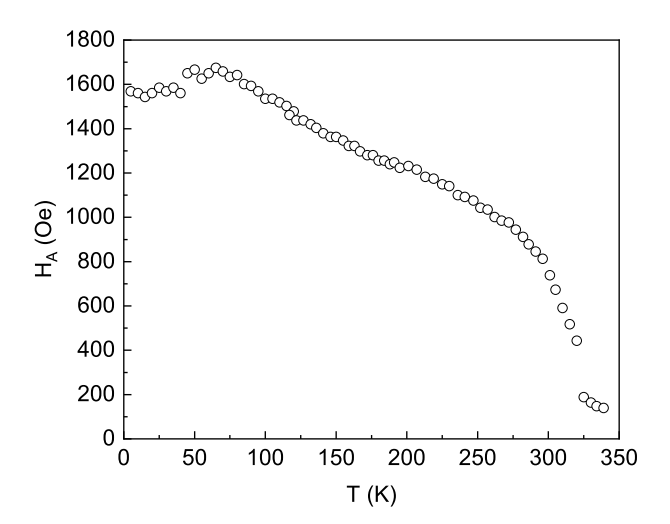


Figure 10. Temperature dependency of anisotropy magnetic field in Ca_{0.25}Sr_{0.5}La_{0.25}Mn_{0.5}Ti_{0.5}O₃ analyzed using the Curie-Weiss law:

$$\chi = \frac{C}{T - \Theta_{\rm CW}},\tag{6}$$

where χ is the magnetic susceptibility, C is the Curie constant, and $\Theta_{\rm CW}$ is the Curie-Weiss temperature [15]. The resulting Curie-Weiss temperature is positive, indicating a transition to a ferromagnetic state at $T \approx 300\,\rm K$ (see Table 2). Using the calculated Curie constant, the effective magnetic moment was determined via the relation:

$$\mu_{\text{eff}} = \sqrt{\frac{3k \cdot C}{N_{\Lambda}}}. (7)$$

The results of the calculations vary with the external magnetic field strength (0.1 and 1 kOe; Table 2). The effective magnetic moment increases with the strength of the external magnetic field, which implies a change in the spin state of the Mn ions. Another possibility is the formation of ferro- or antiferromagnetic regions within the sample under the influence of the external magnetic field.

The theoretical effective magnetic moment was calculated assuming that all Mn ions are in the high-spin state:

$$\mu_{\text{eff}}^{\text{Theor}} = \left(\sum_{i} \left[N_i \cdot g_i^2 \cdot S_i(S_i + 1) \right] \right)^{1/2}, \tag{8}$$

where g is the g-factor, which equals 2 for Mn ions of any valence, and N is a number of Mn³⁺ and Mn⁴⁺ ions determined by XRF analysis.

The obtained value of $\mu_{\text{eff}}^{\text{Theor}}$ is 3.12, which is significantly higher than the experimental values. This indicates either the presence of Mn ions in low-spin states or suppression of the compound's magnetic moment by internal magnetic fields. The latter can explain the growth of the experimental magnetic moment value with increasing external magnetic field strength, as the external field gradually overcomes the internal fields.

The magnetization curves as a function of magnetic field do not reach saturation within the applied field range, exhibiting a value of at most $\pm 1 \mu_{\rm B}$ at 9 T. The saturation magnetic moment

Magnetic properties of high entropy compound $Ca_{0.25}Sr_{0.5}La_{0.25}Mn_{0.5}Ti_{0.5}O_3$

Table 2. The Curie constant, the Curie-Weiss temperature, and effective experimental magnetic moments of Ca_{0.25}Sr_{0.5}La_{0.25}Mn_{0.5}Ti_{0.5}O₃ sample.

H (kOe)	Θ _{CW} (K)	$C (K \cdot emu/mol)$	$\mu_{\mathrm{eff}}(\mu_{\mathrm{B}})$	$\mu_{\mathrm{eff}}^{\mathrm{Theor}}(\mu_{\mathrm{B}})$
0.1	310	0.35	1.67	2 19
1	290	0.6	2.19	3.12

was calculated using the formula:

$$\mu_{\text{sat}} = \sum_{i} (N_i \cdot g_i \cdot S_i), \tag{9}$$

where g is the g-factor, which equals 2 for Mn ions of any valence, and N is a number of Mn³⁺ and Mn⁴⁺ ions determined by XRF analysis, S = 2 for Mn³⁺ and S = 3/2 for Mn⁴⁺. The calculated saturation magnetic moment has value of 1.75 $\mu_{\rm B}$, which is close to the effective magnetic moment value obtained from the magnetic susceptibility measurement at 0.1 kOe.

5. Conclusion

The perovskite-type compound $\text{Ca}_{0.25}\text{Sr}_{0.5}\text{La}_{0.25}\text{Mn}_{0.5}\text{Ti}_{0.5}\text{O}_3$ was synthesized via a solid-state reaction using no fewer than six precursors. It crystallizes in the tetragonal space group I4/mcm with the lattice parameters $a=b=5.48320\,\text{Å},~c=7.74480\,\text{Å},~\alpha=\beta=\gamma=90^\circ$. Magnetization and ESR studies reveal two distinct transitions: one to a ferromagnetic state at $T\approx300\,\text{K},$ and another at $T\approx40\,\text{K}$. The magnetic ions in the compound undergo a valence or spin-state transition under an applied magnetic field, as indicated by the increase in the effective magnetic moment with increasing field strength. The Seebeck coefficient changes sign at approximately $465\,\text{K},$ indicating a change in the charge carrier type. The electronic band gap was calculated to be $\Delta E=269\pm3\,\text{meV}.$

6. Acknowledgments

The work of I.V. Yatsyk was carried out at the expense of a grant from the Academy of Sciences of the Republic of Tatarstan, provided to young candidates of science (postdoctoral students) for the purpose of defending a doctoral dissertation, carrying out research work, and also performing work functions in scientific and educational organizations of the Republic of Tatarstan within the framework of the State Program of the Republic of Tatarstan "Scientific and Technological Development of the Republic of Tatarstan.

References

- Bhattacharya T., Banerjee R. and Maiti T. Physical Chemistry Chemical Physics, 26, 28874-28883 (2024)
- Popov D.V., Batulin R.G., Cherosov M.A., Yatsyk I.V., Chupakhina T.I., Deeva Y.A., Makarchenko A.S., Fazlizhanova D.I., Shustov V.A., Eremina R.M., Maiti T., Journal of Alloys and Compounds, 1009, 176900 (2024)
- 3. Popov D.V., Batulin R.G., Cherosov M.A., Yatsyk I.V., Chupakhina T.I., Deeva Y.A., Eremina R.M., Maiti T., *Magnetic Resonance in Solids*, **25**, 23301-9 (2023)
- 4. Oses C., Toher C., Curtarolo S., Nature Reviews Materials, 5, 295 (2020)
- 5. Zhang R. Z., Reece M. J., Journal of Materials Chemistry A, 7, 22148 (2019)

- Jiang S., Hu T., Gild J., Zhou N., Nie J., Qin M., Harrington T., Vecchio K., Luo J., Scripta Materialia, 142, 116-120 (2018)
- 7. Das R., Sen S., Chowdhury S., Bhattacharya S., Mondal S., Mandal T.K., Gayen A., Mutta V., Seikh M.M., *Journal of Physical Chemistry C*, **129**, 940 (2025)
- 8. Kumar A., Berardan D., Dragoe D., Riviere E., Takayama T., Takagi H., Dragoe N., *Materials Today Physics*, **32**, 101026 (2023)
- Baiutti F., Chiabrera F., Acosta M., Diercks D., Parfitt D., Santiso J., Wang X., Cavallaro A., Morata A., Wang H., Chroneos A., MacManus-Driscol J., Tarancon A., Nature Communications, 12, 2660 (2021)
- 10. Ye S., Zhu J., Zhu S., Zhao Y., Li M., Huang Z., Wang H., He J., *ACS Applied Materials & Interfaces*, **15**, 47475-47486 (2023)
- 11. Shi Y., Ni N., Ding Q., Zhao X., Journal of Materials Chemistry A, 10, 2256 (2022)
- 12. Zhu Y., Liu X., Buckingham M.A., Acharyya P., Guilmeau E., Mehdi B.L., Lewis D.J., Freer R., Journal of the European Ceramic Society, 44, 4666-4679 (2024)
- 13. Joshi J.P., Bhat S.V., Journal of Magnetic Resonance 168, 284 (2004)
- 14. Yatsyk I., Eremina R., Chupakhina T., Deeva Yu., Magnetic Resonance In Solids, 24, 22202 (2022)
- Popov D.V., Batulin R.G., Cherosov M.A., Yatsyk I.V., Yanilkin I.V., Moshkina E.M., Gubaidullin A.T., Fazlizhanova D.I., Eremina R.M., Journal of Alloys and Compounds, 1040, 183213 (2025)
- 16. Nazir G., Rehman A., Hussain S., Algrafy E., Mahmood Q., Mera A., Hegazy H.H., Alharthi S., Amin M.A., *Materials Today Communications*, **31**, 103547 (2022)
- 17. Kholil M.I., Bhuiyan M.T.H., RSC Advances, 10, 43660-43669 (2020)
- 18. Zhang X., Fan J., Xu L., Hu D., Zhang W., Zhu Y., Ceramics International, **42** 1476-1481 (2016)
- 19. Taran S., Sun C.P., Huang C.L., Yang H.D., Nigam A.K., Chaudhuri B.K., Chatterjee S., Journal of Alloys and Compounds, 644, 363 (2015)
- 20. Griscom D., Journal of Non-Crystalhne Solids, 67, 81 (1984)
- 21. Deisenhofer J., Braak D., Krug von Nidda H.-A., Hemberger J., Eremina R.M., Ivanshin V.A., Balbashov A.M., Jug G., Loidl A., Kimura T., Tokura Y., *Physical Review Letters*, **95**, 257202 (2005)